Journal of The Electrochemical Society, **159** (7) D401-D405 (2012)
0013-4651/2012/159(7)/D401/5/$28.00 © The Electrochemical Society

The Effect of Geometric Structure on Photoluminescence Characteristics of 1-D TiO_2 Nanotubes and 2-D TiO_2 Films Fabricated by Atomic Layer Deposition

Yung-Huang Chang,[a] Chien-Min Liu,[a] Chih Chen,[a,z] and Hsyi-En Cheng[b]

[a]*Department of Materials Science and Engineering, National Chiao Tung University, Hsin-chu 30010, Taiwan*
[b]*Department of Electro-Optical Engineering, Southern Taiwan University, Tainan 710, Taiwan*

TiO_2 thin films and TiO_2 nanotube arrays were fabricated on Si and quartz substrates by atomic layer deposition (ALD) with the application of anodic aluminum oxide (AAO) template at 400°C. In particular, the thickness of the film and the wall thickness of the nanotubes can be controlled precisely using ALD technique. The photoluminescence (PL) characteristic of TiO_2 thin films was improved with increased thickness. However, for TiO_2 nanotube arrays, with the decrease of the wall thickness, higher PL intensity was obtained. Compared TiO_2 thin film with TiO_2 nanotube arrays, TiO_2 nanotube arrays exhibited a better performance on PL characteristic due to larger surface area. Owing to larger amount of oxygen vacancies on the surface, compared with the volume factor, surface area was a more important factor that affected the performance of PL characteristics. Therefore, when the volume of TiO_2 nanotube arrays became smaller, the ratio of surface area to volume was increased and the influence from the surface area became the dominating factor on the performance of the PL characteristics.
 [DOI: 10.1149/2.004207jes]

Manuscript submitted January 24, 2012; revised manuscript received March 14, 2012. Published July 17, 2012.

Due to their unique physical and chemical properties, nanostructured materials have attracted considerable number of interests in recent years.[1–10] Among them, TiO_2 nanostructures have become one of the most promising materials for the application of optoelectronic devices due to the following characteristics: variety of growing methods, a high melting point of 1855°C, high thermal and chemical stability at high temperatures, a wide and indirect band-gap semiconductor, high photo-conversion efficiency and photo-stability. Because of these excellent optical properties, TiO_2 has been utilized in many applications including field emitters,[11] dye sensitized solar cells,[12,13] photocatalysis,[14,15] photoelectrochemical water splitting,[16,17] photoelectrochemical generation of hydrogen,[18] photodetectors[19] and gas sensors.[20] In 1972, Fujishima and Honda[21] reported that water can be decomposed directly by irradiating TiO_2 surface with the incident light of wavelengths shorter than 190 nm. In 1991, M. Grätzel et al.[12] fabricated dye sensitized solar cells (DSSCs) using nanocrystalline porous TiO_2 as the electrode to convert solar light to electron-hole pairs. Furthermore, in order to enhance the optical application limited by the innate bandgap (3.2 eV), TiO_2 doped with N,[22] C[23] and S[24] have also been studied. Until now, most of the researches on TiO_2 material were focused on DSSCs, photocatalysis and the modification of material properties in the hope for it to absorb more solar light. Among the studies of optical characteristics of TiO_2 material, photoluminescence (PL) provides important information in understanding the influence of defect levels on the irradiation emission, especially at a material surface.[25] However, a systematic study of photoluminescence on surface condition and the comparison of 1-D and 2-D TiO_2 material are rarely performed, especially for various tubal nanostructures with different tube wall thicknesses.

In this study, we prepared 1-D TiO_2 nanotube arrays and 2-D TiO_2 thin films using AAO template and ALD technology at 400°C in air environment. We then investigate the effect of the geometric nanostructure on the photoluminescence of irradiation emission for various film and tube wall thicknesses. The mechanism of the carriers transitioned from defect levels to valence band is also discussed.

Experimental

To fabricate an AAO template, an Al film of 1 μm in thickness was deposited on P-type (100) silicon or quartz substrate by a thermal evaporation coater. After the fabrication procedure described in an earlier report[26] was performed, we obtained an AAO template possessing an average diameter of about 70 nm, a pore distance of about 95 nm, a height of about 750 nm, and nanopores with an aspect ratio of 10.7. ALD technique was then employed to deposit TiO_2 onto AAO nanopores. Under the operating environment of 1.6×10^{-1} Torr and 400°C, Titanium tetrachloride ($TiCl_4$) and deionized (DI) water were used as the precursors for TiO_2 deposition. Pure Ar gas (99.999%) was used to carrier gas and purge gas, and the reaction is shown as the following:

$$TiCl_4 + 2H_2O \rightarrow TiO_2 + 4HCl \quad (1)$$

The precursors were kept separately in a canister at 30 ± 1°C and 25 ± 1°C, and TiO_2 was deposited onto Si or quartz substrates with or without AAO template in a quartz tube reactor. Each deposition cycle consisted of eight steps, which included $TiCl_4$ reactant entry, pump-down, Ar purge, pump-down, H_2O reactant entry, pump-down, Ar purge, and pump-down. Typical pulse time for the introduction of $TiCl_4$ and H_2O precursors was 1 second. Ar purge time was also 1 seconds. In order to remove the residual reactants and by-products efficiently, 1s pump-down step was added after each step. The deposition cycles of 50, 100, 200, 300 and 700 cycles were chosen to produce TiO_2 thin films with different thicknesses or nanotubes with different wall thicknesses. After the deposition of TiO_2 nanotube arrays on AAO nanopores was completed, TiO_2 film on the top surface of the AAO was removed with mechanical polishing as shown in Figure 2. Then the AAO template was selectively removed by a 0.4 wt% sodium hydroxide (NaOH(aq)) solution. Finally, the self-aligned, equal height and almost equal spaced TiO_2 nanotubes were successfully fabricated.[19]

The nanostructures of the TiO_2 arrays and thin films were examined by a field-emission scanning electron microscope (FESEM, JSM-6500F) and a transmission electron microscope (TEM, JEM-2100F). UV-vis spectrometer (U-3500, Hitachi) was used to measure the light absorption characteristic at 325 nm wavelength for TiO_2 thin film and nanotubes on quartz substrates. Photoluminescence (PL) of TiO_2 nanostructures and thin films on silicon substrate was measured at room temperature, using a continuous beam of He-Cd laser of 325 nm wavelength as the excitation source.

Results and Discussion

Figure 1 shows the TEM cross section of TiO_2 thin film with 50 to 700 deposition cycles. Based on the growth rate of 0.058 nm/cycle, the thickness was 6.6 nm, 8.1 nm, 12 nm, 18.2 nm and 41.1 nm with 50, 100, 200, 300 and 700 deposition cycles, respectively. Figure 1f is the high resolution TEM picture of Figure 1b after 100 deposition cycles, and from the picture, we observed a clear layer of crystalline TiO_2 grown on the top of the native oxide. Furthermore, the lattice spacing was 3.52 Å, which is the distance between (101) planes of the

[z]E-mail: chih@mail.nctu.edu.tw

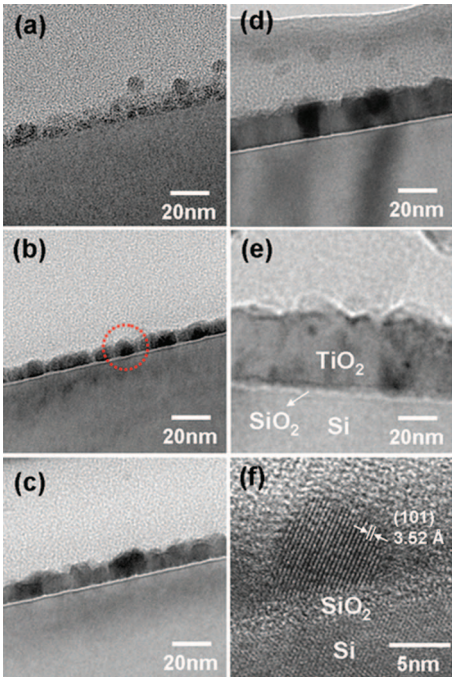

Figure 1. TEM cross section of TiO_2 thin films with deposition cycles of (a) 50, (b) 100, (c) 200, (d) 300 and (e) 700 at 400°C. (f) is the high resolution TEM picture of the dotted circle shown in (b). After 100 deposition cycles at 400°C, a layer of crystalline TiO_2 was clearly observed on the top of the native oxide.

TiO_2 anatase phase.[27] This represents that the precursors, $TiCl_4$ and H_2O, possessed enough energy to overcome the barrier height and form crystalline structures during the reaction at 400°C. In addition, after 100 deposition cycles, the grain size was 8.2 nm, same as the height of the thin film,[28] indicating that the grain size was increasing with increasing thickness of the film.

Figure 2a–2e shows that FESEM cross section of TiO_2 nanotube arrays on AAO templates after deposition cycles of 50, 100, 200, 300 and 700. As the deposition cycle was increased, the nanotube wall thickness was increased and the inner diameter of the nanopores was reduced. In addition, the inner diameter of nanopores seemed to be consistent from the top to the bottom of the nanotubes. It was 21.9 nm at the top and 22.1 nm at the bottom of the nanotubes with 100 deposition cycles, presenting just a minor difference. Figure 2f and the inset in the figure show the cross-sectional and plan-view SEM images of the TiO_2 nanotube arrays deposited at 200 cycles after the removal of the AAO, respectively. The nanotubes are vertical to the Si substrate, and no residual AAO template was observed. The average diameter of the nanotube is about 75 nm, the wall thickness is about 8.8 nm, and the height of TiO_2 nanotube array is about 550 nm. Because the mechanical strength for the tubular structure at cycles less than 100 is not strong enough to support the tubular structures after the removal of the AAO,[29] the PL tests for the tubular structures can be performed only in 700- 300- and 200-cycle conditions. The result confirms the excellent capability for ALD to fill a hole with high aspect ratio because it can precisely control the wall-thickness of TiO_2 nanotube by cycle numbers due to its self-limiting reaction caused by the saturated surface adsorption of reactants. As a result, ALD can produce thin films with high uniformity and provides excellent step coverage. Based on the TEM pictures not shown here,[19] with the growth rate of 0.05 nm/cycle, the wall thicknesses of TiO_2 nanotube arrays were 3.0 nm, 5.3 nm, 8.5 nm, 15.2 nm and 30.7 nm for deposition cycles of 50, 100, 200, 300 and 700, respectively.

In the study of PL characteristic, there are two factors contributing to the intensity of the TiO_2 spectrum. One is called excitation emission, contributed from the transitions of electrons from the conduction band to the valence band, and possesses the wavelength of 388 nm lo-

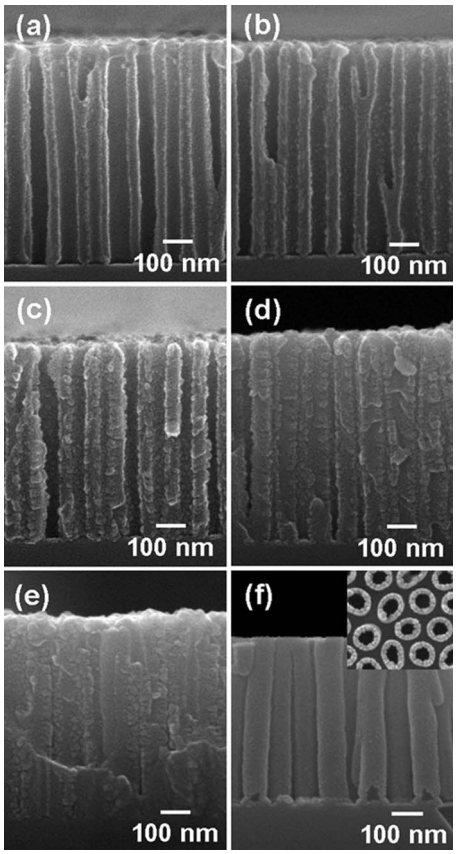

Figure 2. FESEM cross section of TiO_2 nanotube arrays after deposition cycles of (a) 50, (b) 100, (c) 200, (d) 300 and (e) 700 at 400°C. AAO templates have not been removed in the pictures. (f) Cross-sectional SEM image for the TiO_2 nanotube arrays deposited at 200 cycles after the AAO removal. The inset shows the planar SEM image for the nanotubes.

cated in the ultraviolet light region.[30,31] The other is contributed from the defects inside the material, and it is the transitions of electrons from the defect energy level to the valence band, possessing the wavelength between 400∼600 nm located in the visible light region.[30–33] According to the literature,[7,25] the possible defects that can contribute to PL characteristic are oxygen vacancies, titanium interstitials, impurities or defects in the crystal. Among them, the existence of oxygen vacancies is the most accepted source of emission for TiO_2.[25,32,33] The two kinds of oxygen vacancies that can contribute to the PL characteristic in TiO_2 include F centers and F^+ centers. F center represents the neutral oxygen vacancy whereas F^+ center represents oxygen vacancy losing one electrons. The sub-bands contributed from the two kinds of oxygen vacancies, as shown in Figure 3, are located at 465 nm and 525 nm in the PL spectrum, respectively.[30–33]

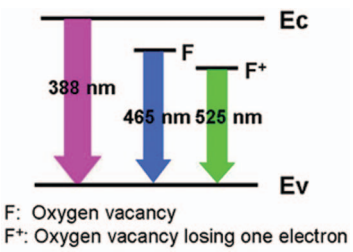

Figure 3. The Energy bandgap diagram of PL characteristic of TiO_2. The excitation emission represents the electron transitions from conduction band to the valence band possessing the wavelength of 388 nm. The transition at 465 nm and 525 nm represent the defect-level transitions from Oxygen vacancies of F center and F+ center to the valence band.

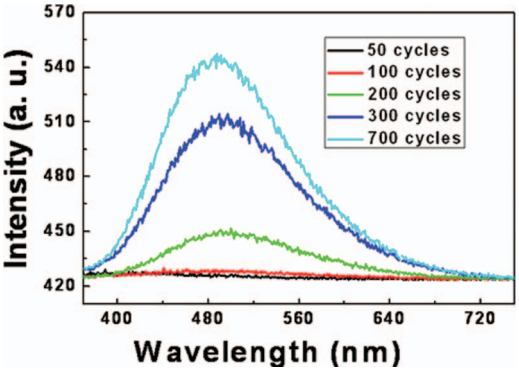

Figure 4. PL spectra of TiO_2 thin film with 50, 100, 200, 300 and 700 deposition cycles.

Figure 4 shows the PL spectra of TiO_2 thin films with 50, 100, 200, 300 and 700 deposition cycles. The sub-band of 488 nm contributed from the excitation emission was not observed because anatase TiO_2 is an indirect bandgap material, and most PL observed is attributed from the transitions of defects in TiO_2. From the PL spectra, we also notice that PL intensity increases with film thickness. In other words, film thickness has a direct relationship with the PL intensity, even though the relationship between the two is not entirely linear as shown in Figure 5. Nevertheless, Figure 5 shows that when the film thickness was increased, light absorption was also increased. Because more electron-hole pairs were generated by the light absorption of the thicker film, the probability of electrons transitioned from the defect energy levels to the valence band also increased, producing a higher PL intensity.

Figure 6 shows the Gauss fitting of PL spectra contributed from oxygen vacancies for TiO_2 thin films with 200, 300 and 700 deposition cycles. The two sub-bands are located at 465 nm and 525 nm in the PL spectrum as mentioned earlier. The intensities of sub-bands decrease with the intensity of the PL spectrum. The detail summary of the PL intensity for the two sub-bands, calculated by the area under the spectra of TiO_2 thin films, is shown in Table I. As observed from Table I, the intensity representing F center was decreasing at a very fast rate with decreasing deposition cycles. The intensity representing F+ center also had a similar trend, but was decreasing at a much slower rate. The ratio of the intensity for F center was 7.1:4.0:1.0 for 700, 300 and 200 deposition cycles whereas the ratio of the intensity for F+ center was 3.9:3.2:1.0 for 700, 300, and 200 deposition cycles. The intensity of F center decreased more rapidly than F+ center was due to the reason that the depletion region on the surface of thin films[34] only contained F+ center. When the thickness of the TiO_2 thin film was decreased, the number of F+ center on the surface was only

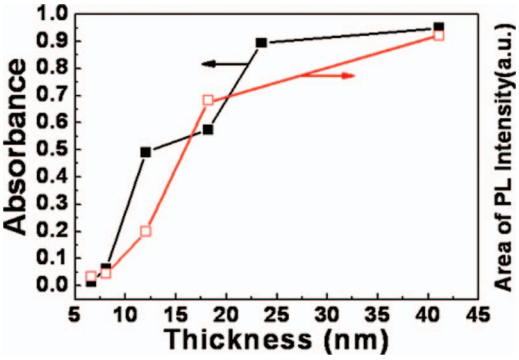

Figure 5. The absorbance vs. area of PL intensity for different thicknesses of TiO_2 thin film. PL was measured at room temperature, using a continuous beam of He-Cd laser of 325 nm wavelength as the excitation source. Absorbance was measured at 325 nm wavelength.

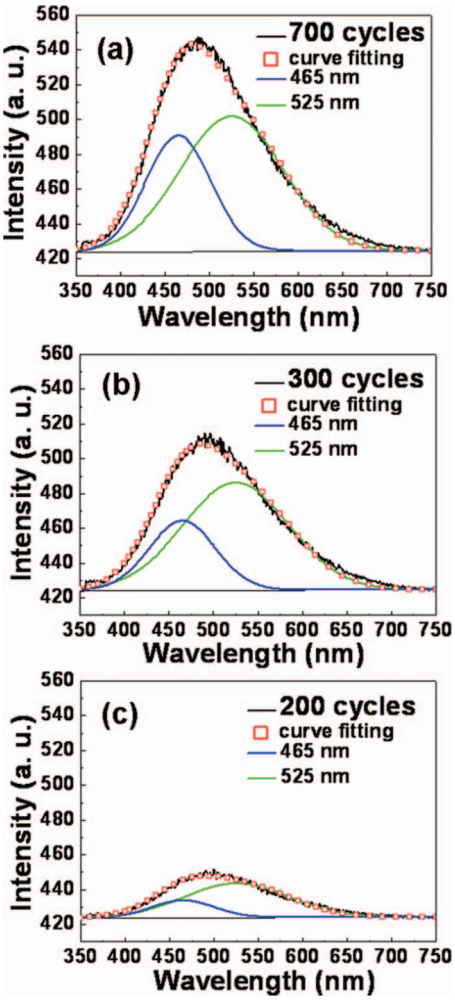

Figure 6. Gauss fitting of PL spectra for TiO_2 thin films with (a) 700, (b) 300, and (c) 200 deposition cycles.

reduced by a small amount. The number of F+ center and F center inside the bulk TiO_2, however, was highly affected by the volume of thin films. This is because when the thickness of the film was reduced, the ratio of surface area to volume was increased. In other words, the value of F+/F became higher and the surface area factor became more important.

Figure 7 shows the PL spectrum of TiO_2 nanotube arrays with 200, 300 and 700 deposition cycles at 400°C. Again, because anatase TiO_2 has an indirect bandgap, the intensity was only contributed from defect levels of oxygen vacancies. As shown in the spectra, TiO_2 nanotubes with 200 cycles seemed to have better PL performance. However, when we compare the absorption spectrum with the PL spectrum, we see that two spectrums had opposite trend. The absorbability of the nanotubes increased but PL intensity decreased with tube wall

Table I. The summary of the PL intensity for sub-bands of F center and F+ center oxygen vacancies calculated by the area under the spectra of TiO_2 thin film.

Cycle	465 nm (F) PL area	525 nm (F+) PL area	F+ F	Surface area Volume
700	6161	11336	1.84	0.024
300	3735	9240	2.47	0.055
200	867	2879	3.32	0.083

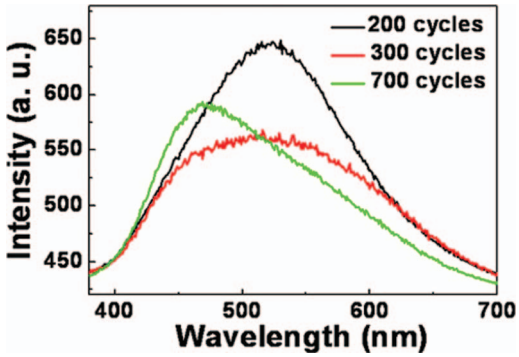

Figure 7. PL spectra of TiO_2 nanotube arrays with 200, 300 and 700 deposition cycles at 400°C.

thickness. As observed in Figure 8, TiO_2 nanotube arrays with 700 deposition cycles showed higher absorbability but lower PL intensity, whereas TiO_2 nanotube arrays with 200 deposition cycles had lower absorbability but higher PL intensity. According to the investigation of Wu et al.[35] on the PL spectra of ZnO nanorods and nanotubes, the tubular structure is advantageous to the optical characteristic because of the higher porosity and larger surface area. Therefore, even though both volume and surface area affect the performance of PL, when the trend of these two factors contradicts with each other, surface area dominates the performance of PL. The reason most likely stems from the fact that the surface area represents a discontinuity of atomic arrangement. Larger surface has higher number of surface defects thus higher number of oxygen vacancies[30–33,35,36] that can contribute to higher intensity for the PL spectrum.

Figure 9 shows the Gauss fitting of PL spectra of TiO_2 nanotube arrays with 200, 300 and 700 deposition cycles. As mentioned previously, the PL sub-bands contributed from F center and F+ center are located at 465 nm and 525 nm, respectively. The PL spectra of TiO_2 nanotubes arrays with 300 and 700 deposition cycles were composed of two sub-bands from oxygen vacancies. The PL spectrum of TiO_2 with 200 deposition cycles, however, only consisted of one sub-band at 525 nm. Based on the trend shown in Figure 9, the PL intensity contributed from F center at 465 nm was decreased with decreasing deposition cycles. Finally, the sub-band represent F center was not observed with 200 deposition cycles. As mentioned earlier, F center and F+ center are located in the bulk of TiO_2 nanotube arrays, and the depletion region on the material surface only contains F+ centers. When the nanotube wall thickness was decreased, the number of F+ center on the surface did not decrease, but the number of F centers and F+ centers inside bulk TiO_2 was decreasing at a fast rate. Therefore,

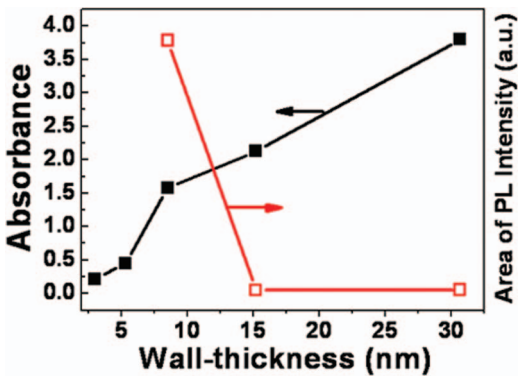

Figure 8. The absorbance vs. area of PL intensity for TiO_2 nanotubes with different wall thicknesses. PL was measured at room temperature, using a continuous beam of He-Cd laser of 325 nm wavelength as the excitation source. Absorbance was measured at 325 nm wavelength.

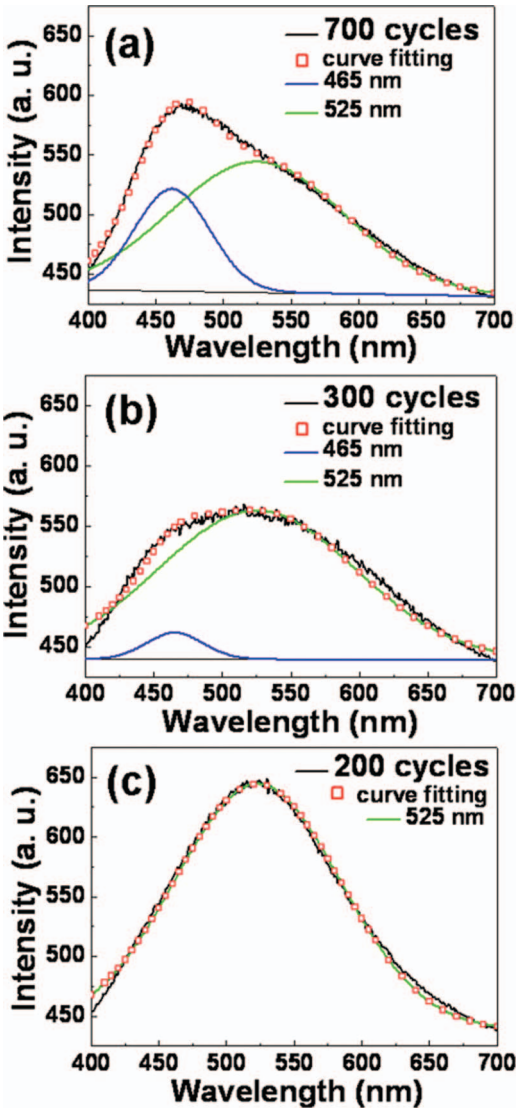

Figure 9. Gauss fitting of PL spectra for TiO_2 nanotube arrays with (a) 700, (b) 300, and (c) 200 deposition cycles.

the total amount of F centers decreased more rapidly than the number of F+ centers, and eventually only F+ centers were observed as the wall thickness was decreased to a certain value as shown in Figure 9c. The detail summary of the PL intensity for the two oxygen sub-bands, calculated by the area under the spectra of TiO_2 nanotube arrays, is shown in Table II. The symbol *S* is the surface area ratio compared with 700 deposition cycles, and the symbol *V* is the volume ratio compared with 200 deposition cycles. Besides, based on the dimensions measured from the TEM and SEM images, the surface area and volume in various conditions were calculated. When the deposition

Table II. The summary of the PL intensity for sub-bands of F center and F+ center oxygen vacancies calculated by the area under the spectra of TiO_2 nanotube arrays.

Cycle	S	V	465 nm (F) PL area	525 nm (F+) PL area	F+ F	Surface area Volume
700	1	1.67	6004	17818	2.97	0.095
300	1.34	1.61	1161	22378	193.4	0.133
200	1.49	1	0	31407	∞	0.237

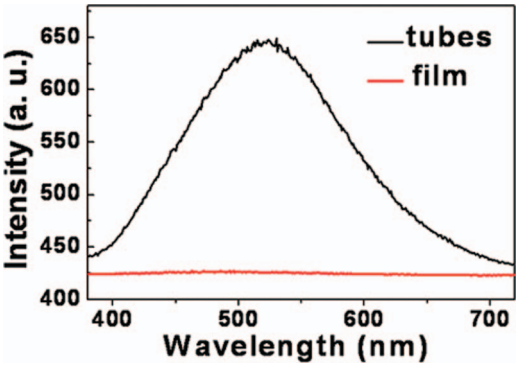

Figure 10. PL spectra of TiO_2 thin film vs. nanotube arrays with 200 deposition cycles.

cycles were decreased, or when the wall thickness was reduced, the ratio of surface area to volume was increased. The surface area then became a more important factor and resulted in higher value of F+/F.

Figure 10 shows the PL spectra of TiO_2 nanotube arrays vs. TiO_2 thin film with 200 deposition cycles. TiO_2 nanotube arrays had a much higher PL intensity than the TiO_2 thin film,[35,36] and the difference was as large as 53 times. If we perform the analysis between the surface areas and the volumes, the surface area of nanotube arrays vs. thin film was 28.1 whereas the volume ratio of nanotubes vs. thin film was 9.9. We can therefore conclude that nanotube arrays have better PL performance than thin films.

Conclusions

In summary, TiO_2 thin films and self-aligned TiO_2 nanotubes were fabricated using ALD technique and AAO templates on Si and quartz substrates. Growth rate of TiO_2 thin film was 0.058 nm/cycle and that of TiO_2 nanotube wall was 0.050 nm/cycle. In particular, by controlling the amount of deposition cycles, the thickness of the film and the wall thickness of the nanotubes can be controlled precisely. For TiO_2 thin film, better PL performance was observed as we increased the deposition cycles and thicknesses. On the contrary, for TiO_2 nanotube arrays, better PL performance was observed for lower deposition cycles and thinner nanotube walls. Both volume and surface area affected the intensity of PL spectrum. However, when the two factors contradicted with each other, surface area became the dominant factor because oxygen vacancies on the surface were the main contribution to the PL characteristic. Therefore, when the amount of materials was decreased, the ratio of surface area to volume was also increased, and the surface factor becomes a more important characteristic to a material's optical properties.

Acknowledgment

The authors thank the National Science Council of the Republic of China, Taiwan, for the financial support in this research under Contract No. NSC-96-2628-E-009-010-MY3.

References

1. Y. Xia, P. Yang, Y. Sun, Y. Wu, B. Mayers, B. Gates, Y. Yin, F. Kim, and H. Yan, *Adv. Mater.*, **15**, 353 (2003).
2. M. H. Huang, Y. Wu, H. Feick, N. Tran, E. Weber, and P. Yang, *Adv. Mater.*, **13**, 113 (2001).
3. Z. W. Pan, Z. R. Dai, and Z. L. Wang, *Science*, **291**, 1947 (2001).
4. Z. L. Wang, *J. Mater. Chem.*, **15**, 1021 (2005).
5. B. P. Zhang, N. T. Binh, K. Wakatsuki, Y. Segawa, Y. Yamada, N. Usami, M. Kawasaki, and H. Koinuma, *Appl. Phys. Lett.*, **84**, 4098 (2004).
6. Z. Y. Yuan and B. L. Su, *Colloids Surf. A*, **241**, 173 (2004).
7. Y. Lei, L. D. Zhang, G. W. Meng, G. H. Li, X. Y. Zhang, C. H. Liang, W. Chen, and S. X. Wang, *Appl. Phys. Lett.*, **78**, 1125 (2001).
8. Y. Wu, R. Fan, and P. Yang, *Nano. Lett.*, **2**, 83 (2002).
9. J. Goldberger, R. R. He, Y. F. Zhang, S. Lee, H. Q. Yan, H. J. Choi, and P. Yang, *Nature*, **422**, 599 (2003).
10. Z. Tang, N. A. Kotov, and M. Giersig, *Science*, **297**, 237 (2002).
11. P. L. Chen, W. J. Huang, J. K. Chang, C. T. Kuo, and F. M. Pan, *Electrochem. Solid-State Lett.*, **8**, H83 (2005).
12. B. O'Regan and M. Grätzel, *Nature*, **353**, 737 (1991).
13. Michael Grätzel, *Nature*, **414**, 338 (2001).
14. S. P. Albu, A. Ghicov, J. M. Macak, R. Hahn, and P. Schmuki, *Nano Lett.*, **7**, 1286 (2007).
15. A. L. Linsebigler, G. Lu, and J. T. Yates, Jr., *Chem. Rev.*, **95**, 735 (1995).
16. G. K. Mor, K. Shankar, M. Paulose, O. K. Varghese, and C. A. Grimes, *Nano Lett.*, **5**, 191 (2005).
17. J. H. Park, O. O. Park, and S. Kim, *Appl. Phys. Lett.*, **89**, 163106 (2006).
18. N. N. Rao and S. Dube, *Int. J. Hydrogen energy*, **21**, 95 (1996).
19. Y. H. Chang, C. M. Liu, Y. C. Tseng, C. Chen, C. C. Chen, and H. E. Cheng, *Nanotechnology*, **21**, 225602 (2010).
20. I. D. Kim, A. Rothschild, B. G. Lee, D. Y. Kim, S. M. Jo, and H. L. Tuller, *Nano. Lett.*, **6**, 2009 (2006).
21. A. Fujishima and K. Honda, *Nature*, **238**, 37 (1972).
22. A. Ghicov, J. M. Macak, H. Tsuchiya, J. Kunze, V. Haeublein, L. Frey, and P. Schmuki, *Nano Lett.*, **6**, 1080 (2006).
23. J. H. Park, S. Kim, and A. J. Bard, *Nano Lett.*, **6**, 24 (2006).
24. T. Umebayashi, T. Yamaki, H. Itoh, and K. Asai, *Appl. Phys. Lett.*, **81**, 454 (2002).
25. N. Serpone, D. Lawless, and R. Khairutdinov, *J. Phys. Chem.*, **99**, 16646 (1995).
26. C. J. Yang, S. M. Wang, S. W. Liang, Y. H. Chang, C. Chen, and J. M. Shieh, *Appl. Phys. Lett.*, **90**, 033104 (2007).
27. C. M. Liu, C. Chen, and H. E. Cheng, *J. Electrochem. Soc.*, **158**, K58 (2011).
28. H. E. Cheng and C. C. Chen, *J. Electrochem. Soc.*, **155**, D604 (2008).
29. Y. H. Chang, S. M. Wang, C. M. Liu, and C. Chen, *J. Electrochem. Soc.*, **157**, K236 (2010).
30. D. Li, N. Ohashi, S. Hishita, T. Kolodiazhnyi, and H. Haneda, *J. Solid State Chem.*, **178**, 3293 (2005).
31. D. Fang, K. Huang, S. Liu, and J. Huang, *J. Braz. Chem. Soc.*, **19**, 1059 (2008).
32. Y. Lei, L. D. Zhang, G. W. Meng, G. H. Li, X. Y. Zhang, C. H. Liang, W. Chen, and S. X. Wang, *Appl. Phys. Lett.*, **78**, 1125 (2001).
33. J. M. Wu, H. C. Shih, and W. T. Wu, *J. Vac. Sci. Technol. B*, **23**, 2122 (2005).
34. X. L. Wu, G. G. Siu, C. L. Fu, and H. C. Ong, *Appl. Phys. Lett.*, **78**, 2285 (2001).
35. C. C. Wu, D. S. Wuu, P. R. Lin, T. N. Chen, and R. H. Horng, *Crystal Growth & Design*, **9**, 4555 (2009).
36. M. Q. Israr, J. R. Sadaf, L. L. Yang, O. Nur, M. Willander, J. Palisaitis, and P. O. Å. Persson, *Appl. Phys. Lett.*, **95**, 073114 (2009).